

A Workstation Based Solar/Stellar Adaptive Optics System

Göran B. Scharmer^a, Mark Shand^b, Mats G. Löfdahl^a, Peter M. Dettori^a, Wang Wei^a

^aRoyal Swedish Academy of Sciences
Stockholm Observatory, SE-133 36 Saltsjöbaden, Sweden

^bCompaq Systems Research Center
130 Lytton Avenue, Palo Alto, CA 94301, USA

ABSTRACT

The microprocessors used in off-the-shelf workstations double in performance every eighteen months. The Swedish Vacuum Solar Tower (SVST) uses off-the-shelf workstations for all aspects of its on-line telescope control and data acquisition. Since 1995 workstation performance has been adequate for a correlation tracker of solar granulation controlling a tip-tilt corrector. In 2000 workstation performance permits the construction of a 20–50 subimage Shack–Hartmann based low-latency adaptive optics system. It is argued that workstations provide a cost-effective, upgradable, low-risk and flexible means of construction of stellar and solar adaptive optics systems.

We give an overview of the adaptive optics system installed at the SVST in May 1999. The system uses a bimorph modal mirror with 19 electrodes from Laplacian Optics. For use with extended targets, such as solar fine structure, cross-correlations with 16×16 -pixel sub-images are used. For use with point sources, a centroiding algorithm is implemented. The work station used is capable of completing all processing required by the adaptive optics system in 0.5 ms (cross-correlations) or 0.3 ms (centroiding), with potential for significant performance improvements.

Keywords: Adaptive optics, Shack–Hartmann, wavefront sensing.

1. INTRODUCTION

The 50-cm Swedish Vacuum Solar Telescope (SVST) in La Palma is widely recognized for its high spatial resolution and excellent image quality. Initially used by a small Swedish community, there has been an increasing demand of observing time from an international community over the past ten years. Associated with this potential for high-resolution imaging, there has been a demand also for a variety of instruments to support such observations. Initial efforts to develop these instruments were heterogeneous and based on a variety of more or less custom made systems. It soon became evident that the staff and budget of the SVST were unable to support and develop this instrumentation further and that a drastically different approach was needed if such efforts were to be successful. During this period, workstations were in increasing use by staff at the SVST. Such machines were becoming ever more powerful and it became natural to investigate whether such technology could be used also for real-time control of instrumentation and for recording data, since this would reduce the requirement for training and maintenance know-how to a minimum.

At the same time the research laboratories of Digital Equipment Corporation (now part of Compaq Computer) were investigating the use of reconfigurable interface and coprocessor boards based on field programmable gate arrays (FPGAs). These boards provide a means of interfacing workstations to high bandwidth external devices that is particularly cost effective in applications that are low volume or whose requirements are ill-defined or evolving. Digital and SVST began a collaboration in 1993 that has led to the construction of a number of control and data acquisition devices, all built around the same basic components of off-the-shelf workstations and reconfigurable interface boards.

Email address: scharmer@astro.su.se.

These instruments include:

- A telescope servo and control system.
- A large frame CCD image acquisition system with on-line frame selection and continuous image preview.¹
- A solar polarimetry system based on two electrically tunable retarders with a single CCD time-multiplexed to receive image data across multiple polarization states² and operating at 60 Hz frame rate.
- A solar polarimetry system based on ferroelectric liquid crystals, built by the Instituto de Astrofísica de Canarias³ and operating at 60 Hz frame rate.
- A low latency correlation tracker for active tip-tilt mirror control and image stabilization.⁴
- A low latency adaptive optics (AO) system, as outlined in Ref. 5 and described in the following sections.

In 2001, the SVST will be replaced by a new solar telescope with one meter diameter.⁶ This telescope will require an AO system to reach its diffraction limit. This paper describes the prototype AO system, used with the SVST. Section two provides motivation for the use of general purpose microprocessors for real-time image processing and compares them to custom developed hardware and specialized Digital Signal Processors (DSP). Section three describes the adaptive optics system and the implementation of the cross-correlation algorithm. Section four describes the adaptive mirror and the calibrations of the AO system. Section five summarizes and discusses some directions for future work. A performance evaluation of the current system will be described in a forthcoming paper.

2. COMPARISON OF GENERAL PURPOSE MICROPROCESSORS, DSPS, AND CUSTOM DIGITAL HARDWARE IMPLEMENTATIONS

Moore's Law has accurately predicted the increase in silicon density of the last 25 years and looks likely to continue to do so for at least the next 10 years. Every 18 months the number of transistors that can be packed into a given area of silicon doubles. This relentless progress of the underlying manufacturing technology has led to ever more powerful semiconductor devices whose computational power is growing exponentially over time.

Moore's law has several consequences for any data acquisition or control system based on a fixed choice of semiconductor technology:

- The system soon becomes obsolete with respect to a system based on newer semiconductor devices. Where development times are longer than a few months, the underlying technology in a system may already be nearing obsolescence before initial deployment.
- Fixed technology systems tend to be expensive or uneconomic to upgrade.
- As the constituent parts become obsolete they may become difficult to obtain, thereby affecting the maintainability of the system.

To maximize the return on our engineering investment, we want to build data acquisition or control systems that can easily migrate to new semiconductor devices as they become available, both to avoid the pitfalls of fixed technology systems, and to realize the performance or cost advantages the newer devices bring. The limited scope of our engineering resources and the difficulty of building custom hardware that can be easily migrated to new semiconductor devices dictate the use of microprocessor based solutions wherever possible. Beyond our compute performance needs, the properties we require in our hardware platform are portability, high performance I/O and scalability.

2.1. DSPs: portability and performance

DSPs are a form of microprocessor that offer an internal organization and specialized instruction set primitives targeted toward the operations that arise in digital signal processing and real-time control. As such they may seem the natural choice for any *processor* based data acquisition or control system. However DSP solutions entail many of the disadvantages of custom hardware development that lead to early obsolescence with no upgrade path to new technology. To maximize performance, DSPs tend to expose the internal architecture of the processor to a much greater extent than does a general purpose microprocessor. As a consequence, it is difficult to write efficient compilers from languages like C to DSPs and so they are often programmed in assembly language. Furthermore, there is limited compatibility in program code of successive generations of DSPs due to the internal architecture changes that accompany new generations.

General purpose microprocessors on the other hand are careful to maintain compatibility between successive generations at the binary machine code level and between different architectural families through the provision of high-level language optimizing compilers which allow efficient applications to be written in a highly portable manner. Meanwhile advances in computer architecture such as caches and superscalar pipelined execution units have rendered general purpose microprocessors as efficient per clock tick as DSPs,⁷

At the same time the clock speed improvements of general purpose microprocessors have substantially outpaced DSPs such that the uniprocessor performance of modern general purpose microprocessor greatly exceeds that of current DSPs. While a number of DSPs can be combined to somewhat mitigate the advantages of the general purpose microprocessor, such combining entails communication overheads and complicates algorithms.

2.2. High performance I/O mechanisms and real-time scheduling

The key feature of DSPs which general purpose processors typically lack is flexible high-speed low-latency I/O facilities for direct interfacing with external instruments. For SVST these facilities are provided by Compaq's *Pamette* reconfigurable interface technology.⁸

The Pamette technology collects several FPGAs (field programmable gate arrays) together on an I/O expansion card and provides a runtime environment for applications to configure and control these FPGAs. Using FPGAs for computation – reconfigurable computing – has recently become a popular idea. Certainly a number of image processing tasks could be done on the FPGAs, but we resist this temptation. By keeping the computation in the host microprocessor, our systems get faster with each new workstation release and they are simpler to develop and enhance. The FPGAs' role is restricted to marshaling data and meeting the most stringent of our real-time requirements.

For less demanding real-time scheduling, modern workstation operating systems provide the ability to assign real-time process priorities and aggressive scheduling policies. On fast microprocessors these facilities are adequate for sub millisecond response.

Figure 1 illustrates the achieved real-time performance with the SVST AO system when wavefront sensing is used with a point target (centroiding). The figure shows the time needed to process each frame during a time interval of two seconds, corresponding to 2000 processed frames. The average time per frame is $282 \mu s$, with a minimum of $272 \mu s$ and approximately 1% of the frames requiring more than $320 \mu s$. This stable performance was achieved while running the AO C-program

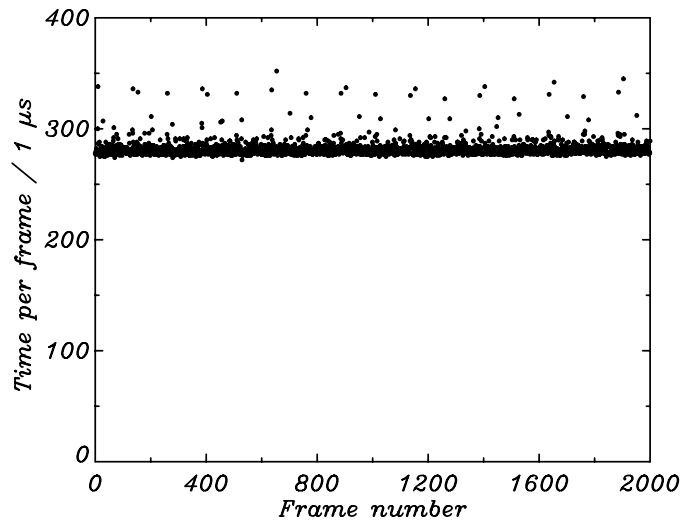


Figure 1. Timing of workstation based AO system when used in centroiding mode

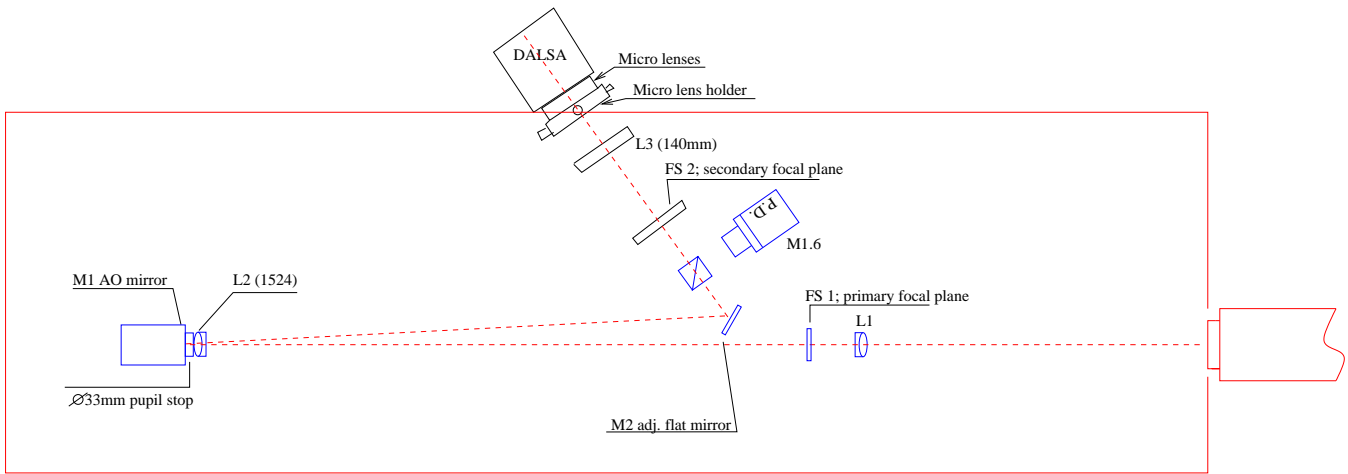


Figure 2. Optical setup. The field lens L1 re-images the 50-cm aperture on the adaptive mirror M1, which is preceded by a lens L2 which re-images the primary focal plane at FS 2. A beamsplitter near FS 2 allows the wavefront to be analyzed simultaneously by a Shack–Hartmann and a phase diversity (PD) wavefront sensor.

at elevated priority under Compaq Tru64 Unix (formerly Digital OSF-1). It demonstrates that demanding real-time systems can be built on standard work station technology using the features present in standard operating systems, contrary to common belief.

2.3. Scalability

It is important to make the distinction between systems that must scale to deliver increased performance in the future versus systems that must scale to deliver a range of performances in a fixed technology. In the former case, semiconductor progress will often provide the necessary performance increases. Moreover, much of the development of such systems can be carried out on hardware with less performance than is required in the operational system, in anticipation of newer, more powerful hardware that we can predict will become available before the scheduled deployment of our system. In the latter case, systems must be constructed to allow a variable number of physical devices to be applied to the computation. Much care is required in the design of such systems if communication between cooperating devices is not to become a bottleneck. Fortunately, our scalability needs are almost always of *future* scalability.

3. DESCRIPTION OF THE AO SYSTEM

3.1. Optical setup

The setup used at the SVST is shown in Fig. 2. The field lens, L1, reimages the telescope pupil onto the pupil stop near the deformable mirror, M1. The primary focus is one focal length (1524 mm) from the collimator lens, L2. A field stop, FS1, in the primary focus protects M2 from excessive heat. When measuring the control matrix of the adaptive mirror, FS1 is replaced by a large pinhole. L2 puts the M1 in collimated space. Both L2 and M1 are slightly tilted, so that the light is reflected at an angle and hits a flat mirror, M2, that deflects the beam towards the sensor part.

A field stop, FS2, at the secondary focus defines the field of view, so that the microlens images do not overlap. FS2 is replaced by a large pinhole for zero-point calibration of the wavefront. The field lens, L3, re-images the M1 pupil stop onto the microlens array. The microlenses re-image the secondary focus onto the detector, a Dalsa 260×260 CCD, reading out 955 frames/s.

A beam splitter deflects part of the light towards the imaging camera, a Megaplus 1.6 with a KAF 1600 CCD. This CCD can be used with a phase-diversity beam splitter, allowing independent measurements of wavefronts and compensation for residual aberrations in solar images as well as independent verification of control matrices and zero-point wavefronts.

3.2. Wavefront sensor

The wavefront sensor consists of a 19-element hexagonal microlens array with appropriate additional optics, as shown in Fig. 2. The measured x,y shifts of the sub-images are used for modal control of aberrations to minimize the effects of the noise in the measured x,y shifts and cross-talk from higher aberrations as described in Ref. 9. In the current setup, approximately 126×140 CCD pixels are used as laid out in Fig. 3. This figure shows the 19 sub-images recorded with a small pore and solar granulation as targets for the wavefront sensor. For all sub-images, except that in the center, 16×16 pixels are used. For the center image, 24×24 pixels are used. This image is used as reference image when doing cross-correlations between the reference image and surrounding sub-images, for determining aberrations higher than tip-tilt, i.e. Zernike¹⁰ 4–19. Additionally, a second reference image which is updated approximately every 20 seconds is used to provide tip-tilt information for image motion correction.

For estimates of displacements of the sub-images relative to the reference image, cross-correlations using the absolute difference algorithm is used. This is done by reading out all possible 16×16 -pixel sub-images from the 24×24 -pixel reference image, taking the absolute value of the difference relative to one of the 16×16 -pixel subimages and accumulating the result. In this way, a 9×9 "correlation" function is constructed, the minimum location of which is found by bi-cubic interpolation. To calculate the correlation function of a single sub-image, therefore requires accumulation of $16 \cdot 16 \cdot 9 \cdot 9 = 20,736$ absolute differences, for all 19 sub-images nearly 400,000 absolute differences need to be accumulated by the CPU.

3.3. Multimedia instruction set extensions

In response to the growing importance of image and video processing in general purpose microprocessors, most major microprocessor architectures have added *multimedia* extensions. These extensions are dedicated instructions to perform parallel manipulation of multiple small integer data items (typically pixels), packed into single machine words. Of particular interest in our context is the Alpha pixel error instruction (PERR). This instruction computes the sum of absolute differences of eight pixels presented in two 64-bit input operands on a full eight bits per pixel and can be issued at the rate of one per machine cycle for the full sum of absolute differences calculation over 8 pixels in current Alpha implementations. At 500 Mhz clock frequency, this implies that up to 4×10^9 absolute differences can be evaluated per second. For the current system, the cross-correlations could in principle be carried out within $100 \mu s$, in practice about $260 \mu s$ are required with the present code and clock frequency and data cache related stalls. Reducing the number of shifts from ± 4 to ± 3 after closing the servo-loop will reduce this time from $260 \mu s$ to $160 \mu s$.

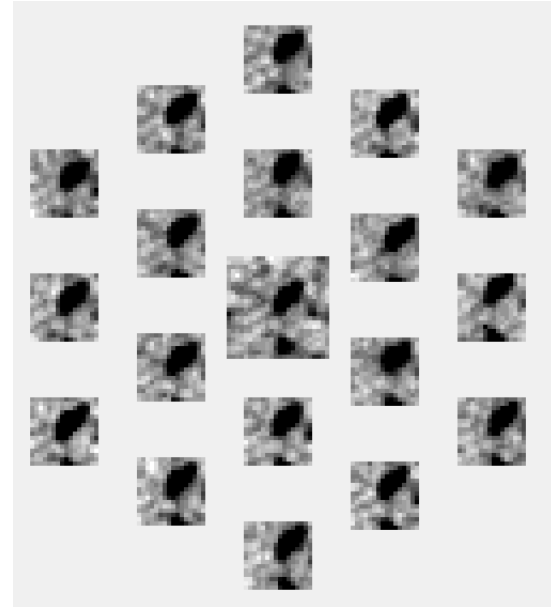


Figure 3. Shack–Hartmann images of solar fine structure (granulation and a small pore). The center reference image has 24×24 pixels, all other sub-images 16×16 pixels. The figure shows the actual location of the sub-images on the CCD.

Table 1. CPU time spent on various tasks in AO code in μs , given both for use on extended targets (cross-correlations) and point-like targets (centroiding). Timing is for 19 sub-images, 18 Zernikes and a 19-electrode bimorph mirror on EV-6 500 Mhz Alpha work station. Each sub-image has 16×16 pixels except the reference sub-image (24×24 pixels). Cross-correlations are done by evaluating all possible ± 4 pixel shifts, centroiding is done over 5×5 pixels centered on the pixel of peak intensity.

Task	Cross corr.	Centroid
Unpacking DALSA 16 bit data	79	79
Flat-field, dark corr, max, min, average intensities	131	131
Average intensity re-normalization	12	–
Sub-image position estimate, cross-correlation	260	–
Sub-image position estimate, centroiding	–	57
Position to Zernike matrix multiply	4	4
Zernike to voltage matrix multiply	12	12
Miscellaneous	4	4
Total time	502	287

3.4. Overall performance

Table 1 summarizes the CPU time spent on various tasks in the AO code. As can be seen in this table, only half of the computing time is spent on cross-correlations. The remainder of the time is dominated by the time needed to unpack the DALSA 16 bit words (2 pixels per word) as well as performing flat-field and dark corrections. In this timing is also included an evaluation of the minimum, maximum and average intensities for each sub-image. These values are used in a rather elaborate scheme which aims at monitoring illumination changes for the different sub-images and continually adjusting the DC levels of the sub-images such that they are equal for all sub-images. Tests and simulations made with our correlation tracker, show that such illumination changes can significantly degrade the accuracy of the position estimates from the cross-correlations unless compensated for.

In the same table can be seen also the timing for the AO system when used with the centroiding algorithm on point targets. With 5×5 pixels used for centroiding and a search over 16×16 pixels for the peak intensity, this time (57 μs) is only 20% of the total time. Most of the time is used on dark correction and flat-fielding as well as evaluating min/max/average intensities which are actually not used in this mode.

It can be noted also that the time needed for matrix multiplications is insignificant with the present system.

The time needed to process one full frame is 500 μs in cross-correlation mode and 290 μs in centroiding mode. It is evident that for night-time use with sub-images smaller than 16×16 pixels and with evaluation of sub-image shifts with fewer than 5×5 pixels using centroid or quad-cell tracking, significant improvements in speed are possible. The performance was obtained on a 500 Mhz Alpha. Already at the time of writing this (March 2000), inexpensive 667 Mhz Alphas are available and higher clock rates, up to 1 Ghz have been announced.

We conclude that inexpensive workstations quite clearly have the capacity to handle all aspects of the computations required by adaptive optics systems for reasonably sophisticated low-latency (1–2 kHz frame rate) AO systems using 50 or more sub-apertures for night-time use and around 35 sub-apertures for use with solar telescopes.

4. ADAPTIVE MIRROR AND CALIBRATIONS

The choice of the bimorph modal mirror from Laplacian Optics Inc. was dictated by the desire of providing the best possible wavefront correction with a small number of electrodes, requirements of high optical quality, low amount of aliasing from high-order mirror modes and the feasibility of simple calibrations of the mirror. In particular,

we wanted to be able to both obtain a control matrix and to calibrate the zero-point wavefront ("flatten the mirror") without having to rely on external wavefront sensors or theoretical calculations of the electrode response. To achieve that, a good match between the geometries of the SH wavefront sensor and the adaptive mirror is required. Fig. 4 shows the mirror electrode geometry. Comparing to the layout of the sub-images in Fig. 3, the relative positions of which correspond to the micro-lens geometry, indicates that this is achieved reasonably well.

4.1. Control matrix calibration

To measure the control matrix, a large pinhole for use with solar light or a small pinhole for use with a laser is inserted at the primary focus, before the adaptive mirror. For each of the 19 electrodes, a low-frequency sawtooth wave of relatively large amplitude is output during approximately 1 s while the AO software determines all Zernikes 2–19, for each frame. This step of the calibration takes a total of 20 s and results in 19,000 wavefront measurements which are stored on disk. When the data has been stored, an off-line reduction program written in an IDL-like but non-commercial language called ANA¹¹ processes the data. The processing consists in using least-squares fits to determine the best linear relation between input voltage and output Zernikes for each of the 19 electrodes. By using 1000 measurements, low-noise measurements are achieved, limited in practice by any small seeing changes within the AO setup during 1 second. This processing takes approximately 10 s, by taking benefit of the high speed of the same workstation as used to control the AO system.

Figure 5 shows the wavefronts for each of the 19 electrodes measured in this way. Comparing to Fig. 4, it is clear that the overall correspondence with the electrode geometry is excellent and that the wavefronts from the different

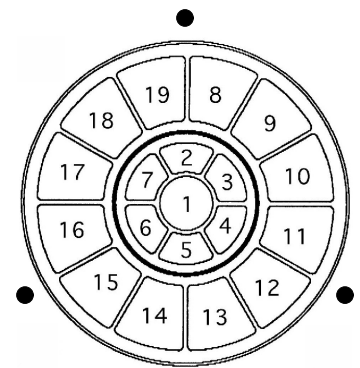


Figure 4. The electrode configuration of the bimorph mirror. The thicker circle inside the outer ring of electrodes indicates the 34 mm pupil diameter. The black dots show the orientations of the three delrin pins holding the mirror. Courtesy of Laplacian Optics, Inc.

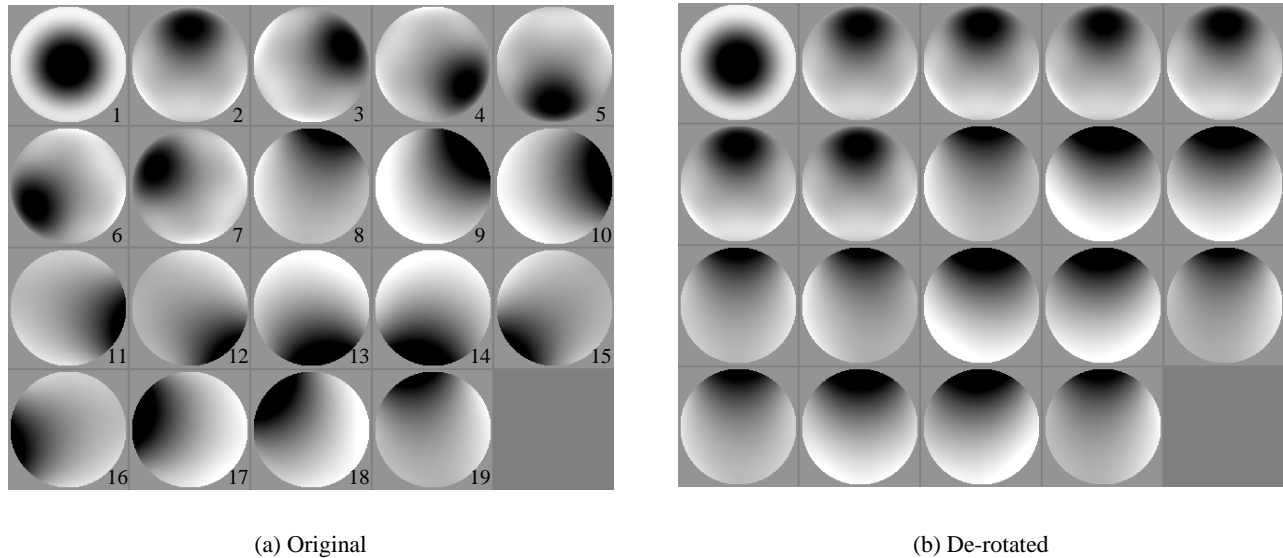


Figure 5. Measured electrode responses (wavefronts) from each of the 19 electrodes, numbered as in Fig. 4 and as obtained with the Shack–Hartmann wavefront sensor. (a) shows the original wavefronts, (b) the same wavefronts after de-rotating. Note that electrodes 8, 11, 12, 15, 16, and 19, which are adjacent to the three mounting pins of the mirror, show smaller response than electrodes 9, 10, 13, 14, 17, and 18.

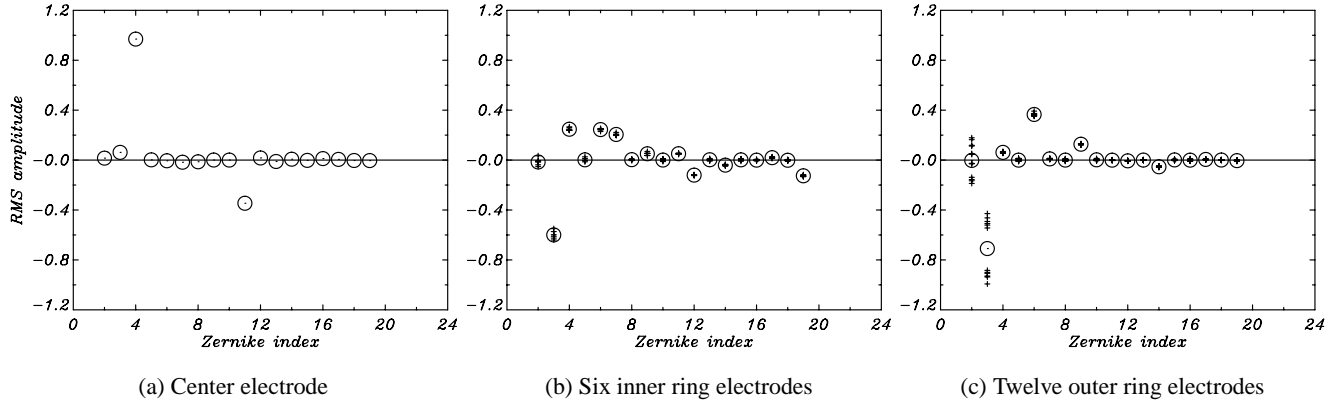


Figure 6. Electrode responses, de-rotated and expanded in Zernike polynomials as obtained directly from calibration with Shack–Hartmann wavefront sensor using Zernikes 2–19. The individual measurements are shown as dots, the averages for each type of electrode as circles. Note the high consistency between the Zernikes measured from the same type of electrode, except the tip–tilt terms (Zernike 2 and 3) for the outer 12 electrodes. Zernike 3 shows two times smaller response for electrodes 8, 11, 12, 15, 16, and 19, which are adjacent to the mounting pins, than for electrodes 9, 10, 13, 14, 17, and 18.

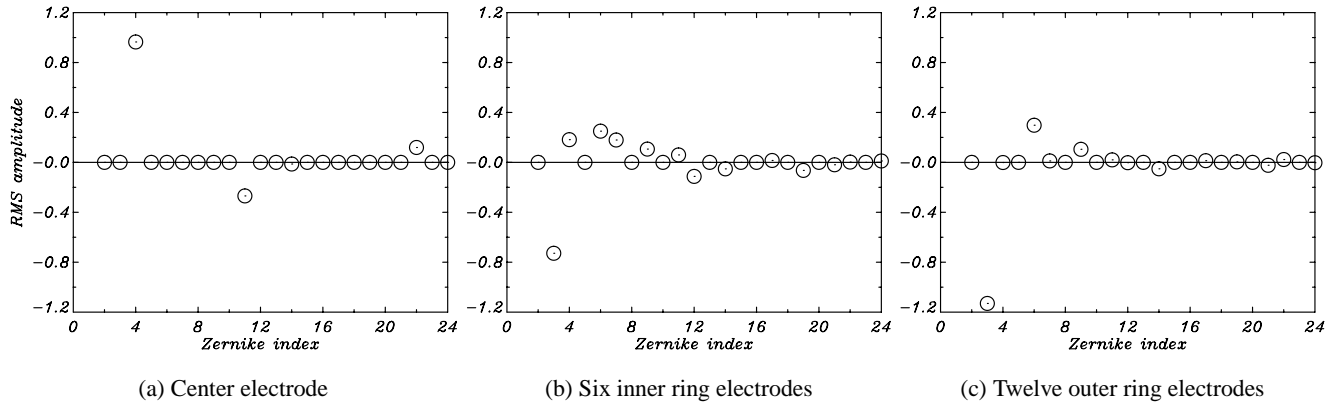
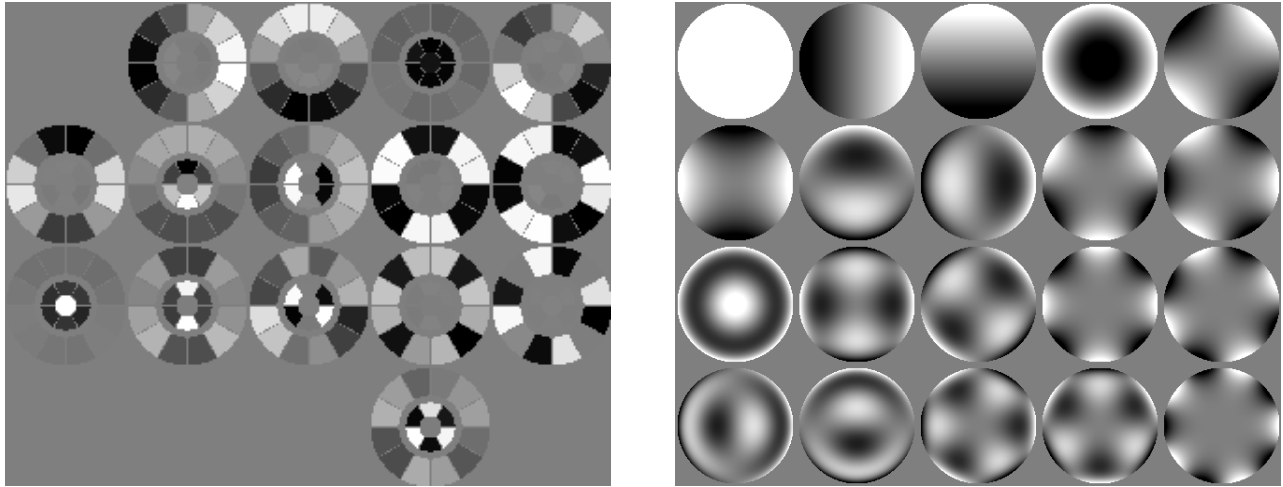


Figure 7. Electrode responses, de-rotated and expanded in Zernike polynomials as obtained from theoretical bi-morph (membrane) model.

electrodes at the same radius are very similar. In order to demonstrate the similarity but also differences, Fig. 5(b) shows the same wavefronts but rotated such as to be symmetric around the y-axis. The wavefronts from the six electrodes of the inner ring appear identical, but there are obvious variations among the electrodes of the outer ring. Decomposing these de-rotated wavefronts into Zernikes is done in Fig. 6. These plots show that the variations in the response of the electrodes in the outer ring is mostly in the tip–tilt terms, Zernikes 2 and 3. Examination of the individual values showed that Zernike 2 has approximately 2 times smaller amplitude for all electrodes which are adjacent to the three delrin mounting pins of the mirror, the locations of which are shown in Fig. 4. It seems likely that these mounting pins also cause minor variations among higher Zernikes, emphasizing the importance of direct measurements of the control matrix.

To verify the validity of the measured electrode responses, a simple membrane model was constructed and solved for, based on the electrode geometry. The surface deformations obtained from these calculations were decomposed into Zernike polynomials to allow direct comparison with the SH based measurements. It is clear from Fig. 7



(a) Control matrix columns.

(b) Zernike polynomials 1–20.

Figure 8. Control matrix columns in graphical form (a) and the corresponding Zernike polynomials for comparison (b). Voltage needed to produce the aberrations corresponding to (b) is encoded as intensity in (a), individually scaled for each aberration. Compare Fig. 4.

that there is good qualitative agreement between the wavefronts obtained from the wavefront sensor and from the membrane model.

By using singular value decomposition (SVD) methods, the response matrix is inverted to give a control matrix, expressing the relation between input Zernike and output voltages. The SVD analysis shows 15 well-determined modes, corresponding to Zernikes 2–15 plus 19. Of the remaining four modes, the two most important are Zernikes 1 (piston) and 21. Fig. 8(a) shows the so-obtained control matrix in graphical form. Here the relative voltages needed to produce a given Zernike aberration is encoded as intensity. In (b) are shown the corresponding Zernike polynomials. Control matrices have also been made from the membrane model and show good qualitative agreement with the empirically determined control matrices.

Our conclusion is that the AO system allows probably excellent control matrices to be determined without relying on external wavefront sensors or calculations. However, direct verifications using an independent wavefront sensor are needed to actually demonstrate this. We are planning to do this with phase diversity, using a procedure established in Ref. 12.

4.2. Zero-point wavefront calibration

The zero-point calibration of the wavefront sensor determines the ultimate wavefront error achievable in closed loop. This calibration is made simply by inserting a large (with solar light) or small (with laser) pinhole at the secondary focus and measuring the relative positions of the sub-images. The positions obtained during this calibration are then subtracted from the relative positions of the sub-images when in closed loop.

Verification of the goodness of this calibrations have been done by using an imaging CCD with a phase diversity wavefront sensor, by splitting off light using a cube beam splitter near the secondary focus and using a very small pinhole at primary focus. Such measurements were made during the development of the system in Stockholm and indicated wavefront errors of approximately 1/40 wave rms. These very low rms wavefront errors were verified with direct measurements of Strehl ratios for the focused images. Although these measurements have not yet been repeated in La Palma, it is obvious from the clean appearance of the diffraction image of the focused pinhole images,

that small systematic wavefront errors are achievable. This is in part due to the excellent optical quality of the bimorph mirror and to the fact that the SH wavefront sensor can measure nearly all the aberrations that the mirror can produce.

4.3. Other calibrations

In order to enable as good a characterization of the system as possible and direct verification of its performance, two other pieces of software have been added. The first consists in running through a large number of unit pulses on a given electrode, with randomly chosen lengths. By accumulating and processing such data, the complete servo response, amplitude and phase shift as function of frequency can be measured. Finally, a simple addition of the AO software was used to allow a hardware measurement of the time delay. The modification to the software consisted in an option to output the measured average intensity as voltage on one of the electrodes. By using a pulse generator, a photo diode and a photo-cell, this allows the computational delay to be measured on an oscilloscope by comparing the output signal from the AO system with that of the photo diode.

4.4. Diagnostics

One of the advantages of a workstation-based AO system is the low cost of adding memory for storing various output data from the AO system and the ease and speed by which such data can be processed off-line. When in closed loop, the AO system keeps all measured sub-image positions, Zernikes, output voltages, as well as timing information for the last 20 seconds in memory. In addition, all sub-images processed during the last 10 seconds are kept in memory. By stopping the AO closed loop, this data is automatically stored on disk. This allows analysis of any problem or unexpected behavior of the AO system as well as evaluation of its performance. Fig. 9 shows a plot of atmospheric and compensated power spectra for one such 20 s long sequence. These power spectra, obtained with a pure I-servo, indicate reasonably good suppression of all Zernikes, except tip-tilt. Other tests obtained in different conditions point to the need for improving bandwidth, either by a faster servo or by increasing the frame rate of the CCD. From the timing of the present system, processing at 2 kHz frame rate should be possible.

5. DISCUSSION

In this paper we have presented a new approach to adaptive optics control system. By using standard workstation technology, low-latency (1–2 kHz frame rate) correction of 35–50 or more aberrations is possible with current technology. Among the advantages of the proposed system are ease of development, future compatibility, future performance upgrades as well as the ease by which system performance can be monitored and analyzed. Last but not least, a single workstation eliminates I/O bottlenecks and allows high performance, limited essentially by the processor.

The SVST system uses a high-quality modal bimorph mirror, matched to a SH wavefront sensor. This allows accurate determinations of both the control matrix and the zero-point wavefront, both of which are necessary for efficient AO systems.

The current AO system was used in 1999 for recording scientific data. It is currently being evaluated and its software improved. In particular, the reference image will be chosen from an earlier exposed frame, to allow full processing of the sub-images on the fly as they are stored in the workstation memory. This will reduce latency. In addition, a smaller reference image will be used to enable more efficient use of the CCD pixels, most of which are un-used in the present system (cf Fig. 3). A faster servo will be implemented to improve bandwidth. An important issue concerns the proper handling of frames where one or more sub-images are blurred enough that sub-image shifts cannot be estimated. This requires reconstruction of the wavefront with missing data. In the present system, this opens the servo-loop temporarily.

Based on the experience with this system in the summer of year 2000, the AO system for the new 1-meter telescope will be developed. This will have 37 electrodes and a SH array with 37 sub-images, matched to the

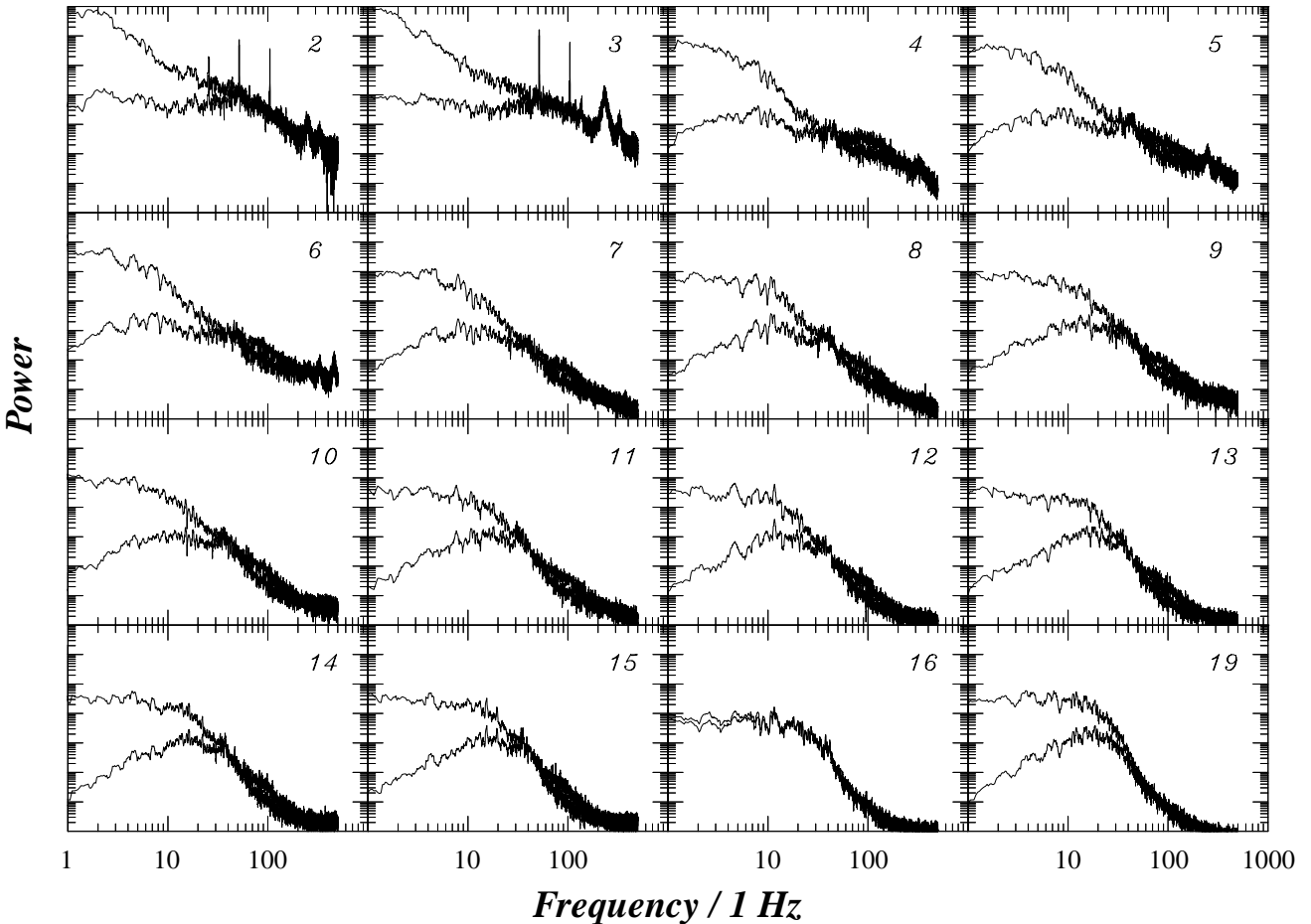


Figure 9. Power spectra for Zernikes 2–16 plus 19. Shown are both atmospheric and residual power for the corrected Zernikes 2–15 and 19 plus the uncorrected Zernike 19. The data were obtained with a pure integrating servo and a frame rate of 955 Hz.

electrode geometry. We believe that such a system can be operated at 2 kHz frame rate on a work-station with a single CPU, by taking advantage of higher clock frequencies of coming workstations and code improvements.

Shack–Hartmann wavefront sensing using cross-correlation techniques is necessary for solar AO but is of interest also for observations of planets and for evaluation of anisoplanatism of seeing. Such observations are planned for the new telescope.

ACKNOWLEDGMENTS

We thank Laplacian Optics Inc. for their efforts in producing an excellent mirror, for numerous valuable discussion and also for providing Fig. 4. The D/A converter connecting the computer to the high-voltage amplifier was made by workshop personnel at the Kiepenheuer-Institut für Sonnenphysik in Freiburg, Germany. The Swedish Vacuum Solar Telescope is operated on the island of La Palma by the Royal Swedish Academy of Sciences in the Spanish Observatorio del Roque de los Muchachos of the Instituto de Astrofísica de Canarias. We finally want to acknowledge stimulating discussions with Thomas Rimmele.

REFERENCES

1. M. Shand, “Flexible image acquisition using reconfigurable hardware,” in *Proc. the Third Annual IEEE Symposium on FPGAs for Custom Computing Machines*, K. L. Pocek and P. M. Athanas, eds., 1995.

2. M. Shand and L. Moll, "Hardware/software integration in solar astronomy," in *FPGAs for Custom Computing Machines (FCCM'98)*, K. Pocek and J. M. Arnold, eds., IEEE Computer Society Press, 1998.
3. V. Martinez Pillet, M. Collados, J. Sanches Almeida, V. Gonzalez, A. Cruz-Lopez, A. Manescau, E. Joven, E. Paes, J. J. Diaz, O. Feeney, V. Sanchez, G. B. Scharmer, and D. Soltau, "LPSP & TIP: Full stokes polarimeters for the Canary islands observatories," in *High Resolution Solar Physics: Theory, Observations and Techniques*, T. Rimmele, R. R. Radick, and K. S. Balasubramaniam, eds., Proc. 19th Sacramento Peak Summer Workshop, ASP Conf. Series vol. 183, p. 264, 1999.
4. M. Shand, W. Wei, and G. Scharmer, "3.8 ms latency correlation tracker for active mirror control based on a reconfigurable interface to a standard workstation," in *Field Programmable Gate Arrays (FPGAs) for Fast Board Development and Reconfigurable Computing*, J. Schewel, ed., vol. 2607 of *Proc. SPIE*, pp. 145–154, 1995.
5. M. Shand, G. B. Scharmer, and W. Wei, "Correlation tracking and adaptive optics control using off-the-shelf workstation technology," in *High Resolution Solar Physics: Theory, Observations and Techniques*, T. Rimmele, R. R. Radick, and K. S. Balasubramaniam, eds., Proc. 19th Sacramento Peak Summer Workshop, ASP Conf. Series vol. 183, p. 231, 1999.
6. G. B. Scharmer, M. Owner-Petersen, T. Korhonen, and A. Title, "The new Swedish solar telescope," in *High Resolution Solar Physics: Theory, Observations and Techniques*, T. Rimmele, R. R. Radick, and K. S. Balasubramaniam, eds., Proc. 19th Sacramento Peak Summer Workshop, ASP Conf. Series vol. 183, p. 157, 1999.
7. L. C. Stewart, A. C. Payne, and T. Levergood, "CRL technical report 92-10." <http://www.crl.research.digital.com/>, 1992.
8. Compaq, 1998. <http://www.research.digital.com/SRC/pamette>.
9. G. B. Scharmer and H. Blomberg, "Optimized Shack–Hartmann wavefront sensing for adaptive optics and post processing," in *High Resolution Solar Physics: Theory, Observations and Techniques*, T. Rimmele, R. R. Radick, and K. S. Balasubramaniam, eds., Proc. 19th Sacramento Peak Summer Workshop, ASP Conf. Series vol. 183, p. 239, 1999.
10. R. J. Noll, "Zernike polynomials and atmospheric turbulence," *Journal of the Optical Society of America* **66**(3), pp. 207–211, 1976.
11. R. A. Shine, L. Z. Porter, Z. Frank, J. B. Gurman, D. Pothier, and S. Ferguson, *A User's Guide to ANA*. Lockheed Palo Alto Research Laboratory, 1988. See also <http://ana.lmsal.com>.
12. M. G. Löfdahl, G. B. Scharmer, and W. Wei, "Calibration of a deformable mirror and Strehl ratio measurements by use of phase diversity," *Applied Optics* **39**(1), pp. 94–103, 2000.